

Article

Comparison between Laser and Stamping without Die (SWD) for Micro Tapered Hole Forming

Yung-Chou Hung ^{1,†}, Yuan-Jen Chang ^{1,*}, Chia-Lung Kuo ^{1,†}, Jin-Chen Hsu ¹ and Chao-Ching Ho ²

¹ Department of Mechanical Engineering, National Yunlin University of Science and Technology, Yunlin 64002, Taiwan; g9911803@yuntech.edu.tw (Y.-C.H.); kuocl@yuntech.edu.tw (C.-L.K.); hsuyc@yuntech.edu.tw (J.-C.H.)

² Department of Mechanical Engineering, National Taipei University of Technology, Taipei 10608, Taiwan; hochao@mail.ntut.edu.tw

* Correspondence: changy@yuntech.edu.tw; Tel.: +886-5-534-2601 (ext. 4129)

† These authors contributed equally to this work.

Academic Editor: Chien-Hung Liu

Received: 8 December 2015; Accepted: 26 February 2016; Published: 15 March 2016

Abstract: The forming of a micro tapered hole is based on nanosecond pulsed laser processing, which conforms to fast processing time and high throughput; however, the microhole quality should be improved. Micro stamping is a technology providing high precise size and speed. The greatest difficulty in forming a microhole by micro stamping is the precision alignment of the punch head to the lower die. In order to overcome the difficulty, we proposed a concept of stamping without die (SWD). Without a lower die, the tapered punch head was directly applied to the workpiece for micro stamping, and a thicker workpiece surrounding the punching area provides a better support to the stamping process. Thus, a successful forming of micro tapered holes is completed. The micro tapered hole depth is 300 μm , and the maximum ratio of inlet to outlet diameter is 18:1. In order to reduce the number of experiments, the finite element analysis software DEFORM-3D was used for forming analysis. The simulation forecast result was compared with the experimental processing, which was well validated. Under different experimental parameters of laser energy and defocusing distance, drilling results by two methods show that the microhole quality by stamping process is better than by laser processing.

Keywords: micro stamping; stamping without die; micro tapered hole; DEFORM-3D; laser processing

1. Introduction

The back covers of consumer electronics products, such as mobile phone, tablet Personal computer (PC) and so on, are required of microholes. The microholes are tiny, but light could pass through them. Without damaging the aesthetic sense of mobile device design by using microperforation illumination technology, the micro holes provide indication functions or replace the input function of keyboard or mouse. The tapered microhole offers higher light extraction efficiency and better illumination uniformity. The current microhole processing methods include laser processing, electro-discharge machining, micro stamping, and wet etching. Among these processing methods, the electro-discharge machining has higher machining accuracy and lower surface roughness, but the processing rate is low. Thus, it is not suitable for mass production. The wet etching process could remove the surface material selectively or globally at the highest etching rate with the best cost effectiveness, but is limited to the specific materials. Meanwhile, the following pollution is always an issue.

In copper and aluminum alloy microhole processing, the laser processing and micro stamping are better choices in terms of machining efficiency, and both processing methods have their own merits and demerits. The laser drilling results in high depth-diameter ratio and machining efficiency. It

can implement high speed drilling, especially applicable to large quantity and high density drilling without tool wear. Due to the Gaussian beam and the effect of defocusing, the microholes by laser drilling are mostly tapered holes [1]. The laser drilling utilizes the high power density of laser to vaporize the workpiece rapidly, and then the melted material is extruded by the surplus pressure of vapor to form holes. As it is a thermal ablation process, the pulsed laser processing is likely to result in char black, molten slag and material deterioration [2,3]. This study uses Nd:YAG laser for drill experiment.

In the application of micro stamping, Masuzawa *et al.* developed the wire electro-discharge grinding (WEDG) mechanism in 1985, which was used in micro-discharge machining, and the microelectrode was created successfully [4]. This technology was also used to make micro punches for micro stamping [5,6]. Grinding technology [7,8] or reverse-electrical discharge machining (EDM) [9] can be used for making a micro punch as well. In this study, we uses reverse-EDM for creating a micro punch. The major problem in making a microhole by micro stamping is the precision alignment of the punch and lower die, which creates bottleneck in current micro punching. While this issue can be overcome by guide pin [10] or image alignment [11], it remains complicated for mold design. Therefore, this study proposes a stamping without die (SWD), where a higher moment of inertia is produced by a thicker sheet, thus, overcoming the bending moment generated by the stamping process. Micro stamping is a micro forming techniques. This plastic forming considers complex structural mechanics and material problems. In recent years, regarding plastic forming analysis, many studies have used finite element analysis software DEFORM-3D to analyze mold wearness, and the flow of material in molds. According to the simulation results, the simulation and experiment are matched well [12–15]. In order to study the feasibility of the proposed process, and find the optimal experimental parameters quickly, the DEFORM-3D is used to predict forming and loading in our micro stamping process. The simulation result can used in the experiments.

The experimental setup of micro stamping is as shown in Figure 1a. The whole setup is on an engraving EDM machine (Sodick AP1L, Baginton Coventry, UK). The punch head is affixed to the Z-axis. Figure 1b shows the schematic diagram of the holder fixing workpiece. The design concept is that the workpiece is fixed by screws and the central part of workpiece is suspended. Figure 1c shows the tapered punch for stamping, which is made by reverse-EDM. A 0.2 mm diameter is drilled in the brass electrode, and then ψ 2 mm Tungsten Carbide (WC) is used for reverse-EDM [9].

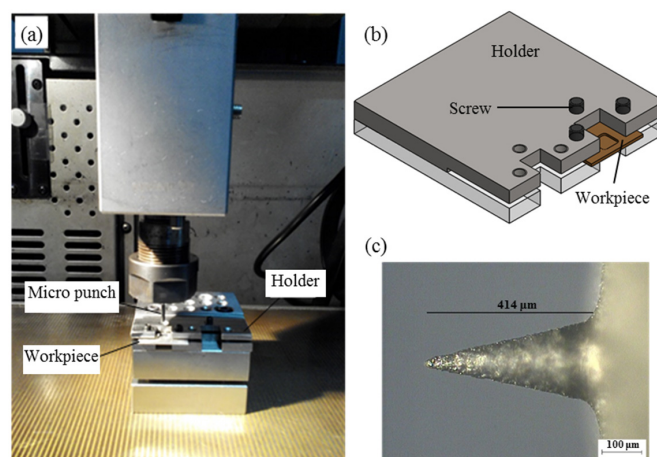


Figure 1. Micro stamping mechanism without a lower die (a) experimental setup (b) schematic diagram of holder (c) micro punch after reverse-EDM (electrical discharge machining). Scale bar = 100 μ m.

In order to discuss the difference between microholes made by laser and micro stamping, a sample with a thickness of 300 μ m is used for laser drilling.

2. Finite Element Software DEFORM-3D

2.1. Computer Aided Design Geometric Modeling

The workpiece and support base are both put in the simulation analysis in order to simulate the buckling effect generated by the designed mechanism. Meanwhile, in order to reduce the number of grids, the DEFORM-3D grid fining function is used for contacting area of the punch head and workpiece. The DEFORM-3D grid fining function for the punch and workpiece are as shown in Figure 2. The minimum edge length in grid fining is 0.001 mm.

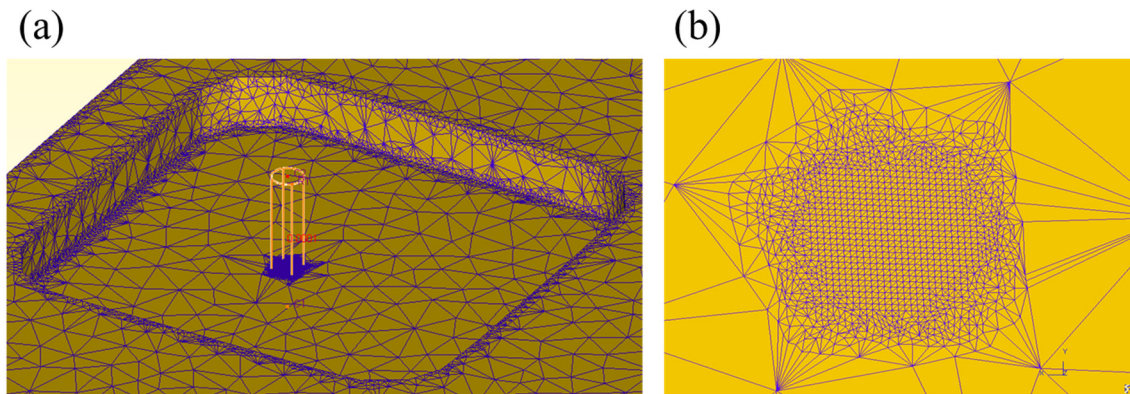


Figure 2. Schematic diagram of workpiece with fine mesh elements (a) mesh refinement (b) partially enlarged mesh.

Since the mesh element number influences the simulation time and result, the grid convergence analysis is applied before simulation. Convergence analysis is based on the Z-axis loading. When the difference between this loading and previous loading is less than 0.1%, it means the convergence has been reached. The mesh element number is set as 50,000–150,000 with an increment of 10,000. The analysis result shows that when the mesh element number reaches 100,000, the load difference is less than 0.01%, and the result has converged. The mesh element number is 100,000 for the subsequent simulation.

First, Solidworks was used to build the entire model for stamping, including the punch head, the workpiece and the support base, as shown in Figure 3. Since this study aims at the process of micro stamping without lower die, the lower die is replaced by a support base. Therefore, the effect of support base bearing distance on the workpiece must be considered. First, CAD software, Solidworks (Version 2015, Dassault Systèmes SOLIDWORKS Corporation, Massachusetts, MA, USA, 2014), is used to draw the punch, workpieces, and lower die size for stamping. The geometry of stamping model is as shown in Figure 3. In this process of SWD, the deformation or buckling of workpieces resulted from the support base is examined. The support base is an 8 mm × 8 mm □-shaped structure. There are two types of workpieces, one is a 0.3 mm thick flat plate; the other is a 1 mm thick flat plate with a groove. The groove size is 6 mm × 6 mm and 0.7 mm deep. Three punch head angles are used, 24°, 54° and 90°. The simulation parameters are listed as shown in Table 1.

Table 1. Simulation parameters of DEFORM-3D.

Parameter	Condition
Workpiece	Al6061
Punch angle	24°, 54°, 90°
Workpiece/Die	Plastic/Rigid
Stamping speed	0.5 mm/min
Stamping depth (Z)	0.38 mm

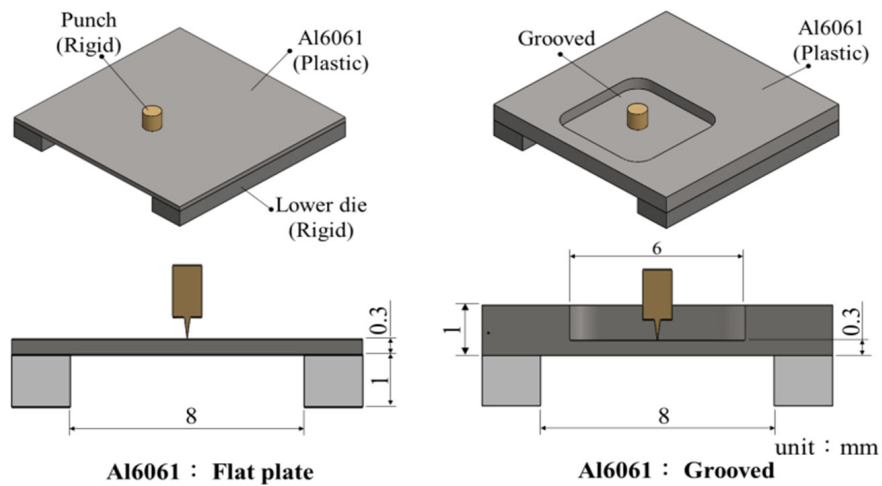


Figure 3. Stamping model specification.

2.2. Simulation Results and Discussion

The simulation results of SWD are shown in Figure 4. Figure 4a shows the result of flat-plate workpiece, while Figure 4b shows the result of grooved workpiece. According to the simulation results, when the stamping depth is 0.38 mm at the same punch head angle with flat plates, the workpiece is largely bent, and the workpiece is unperforated. When the workpiece is grooved and the punch angle is 24° , the workpiece is perforated. No buckling is observed, and only deformation around the outlet is shown in the simulation results. However, the workpiece cannot be perforated as the punch angle increases, and it is largely bent.

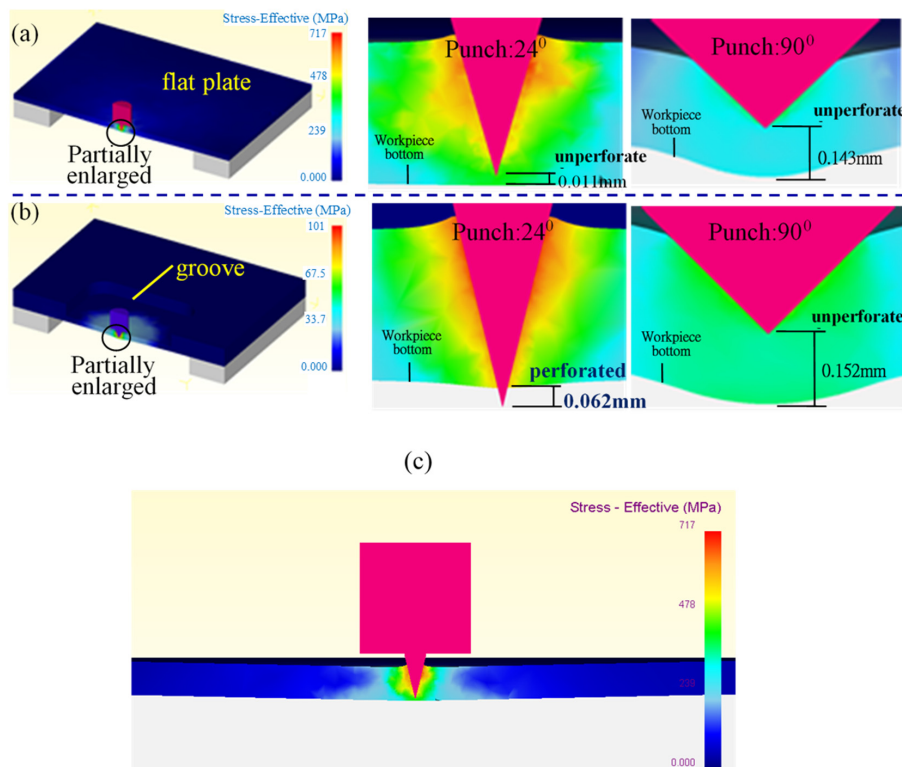


Figure 4. Schematic diagram of workpiece shape/punch angle in punch forming (a) workpiece-flat plate (b) workpiece-grooved (c) deflection of flat plate with a 24° punch head.

This phenomenon is analyzed in the view of mechanics, where the lower die supporting the workpiece is an 8 mm × 8 mm □-shaped groove, and the distance between the application point to the bearing point is very large, which results in a very large bending moment. In stress analysis, the area other than the grooving increases the moment of inertia due to a thicker sheet. This groove contributes to enhancing the punching effect. The relationship between stamping depth (stroke) and punch load is as shown in Figure 5. The punch load is relatively high with a flat plate, and because the tapered punch is V shaped, the lateral force on the punch increases as the workpiece bends (as shown in Figure 4c), and the punch load is high.

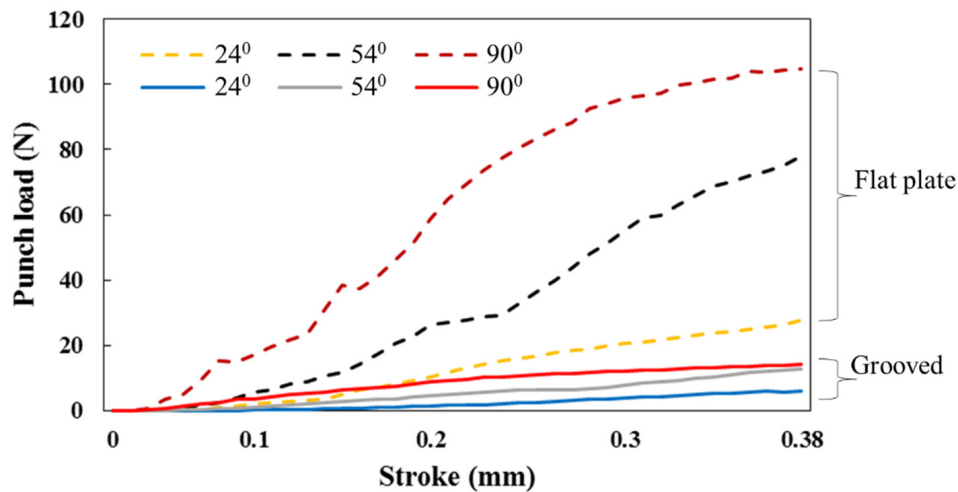


Figure 5. Relationship between stamping depth (stroke) and punch load.

When the workpiece is grooved, the punch at 24° has good punching result. The microhole forming process is as shown in Figure 6. When the stamping depth is 0.34 mm, the workpiece begins to be perforated, and the outlet diameter increases with the stamping depth. While the outlet is slightly bent, it is restricted to the nearby area of the outlet. This result can predict the relationship between stamping depth and perforation. The simulation results will be compared with experiments in the next section.

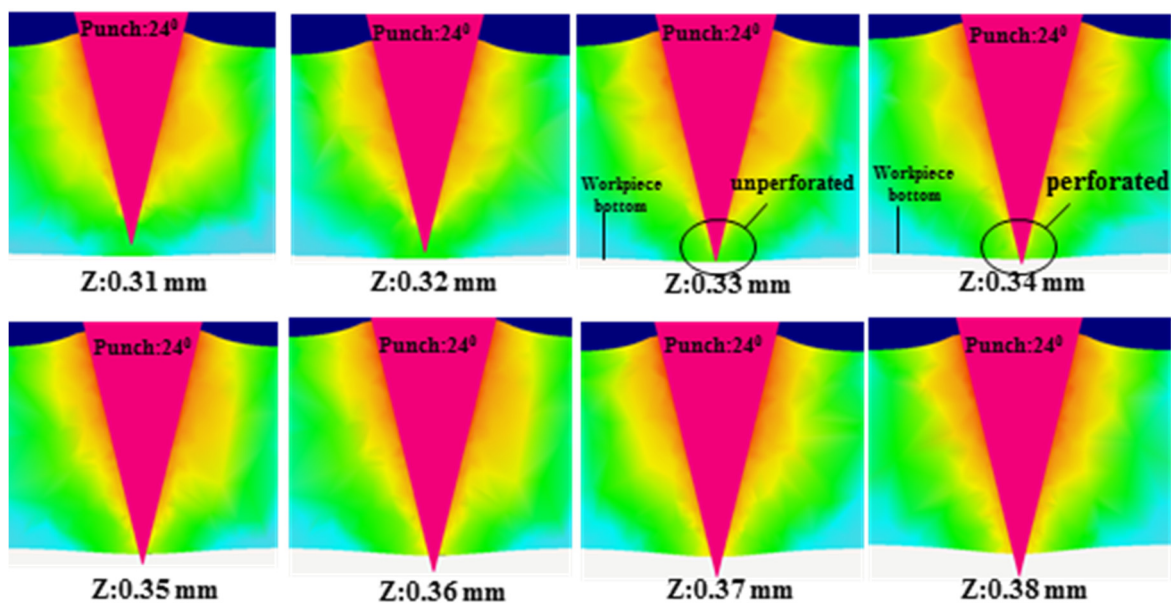


Figure 6. Stamping depth/punch forming relationship simulation analysis.

3. Experimental Method and Procedure

3.1. Micro Stamping

DEFORM-3D Version 6.1 (Scientific Forming Technologies Corporation, Ohio, OH, USA, 2007) is used to simulate SWD, thus, the grooved workpiece and punch head angle (24°) has shown a better result. The simulation results show that the microholes are easier to form as the punch head angle decreases. Therefore, this experiment uses a punch at a small angle for micro stamping on the grooved workpiece.

The processing parameters for the micro stamping experiment are as shown in Table 2. The workpieces are Al6061 and C2680. The workpiece size is $25\text{ mm} \times 25\text{ mm} \times 1\text{ mm}$, and the groove size is $6\text{ mm} \times 6\text{ mm}$ with a depth of 0.7 mm . The micro punch head is made by reverse EDM, the tapered angle is 23.5° , and the length is $414\text{ }\mu\text{m}$, as shown in Figure 1c.

Table 2. Micro stamping parameters.

Parameter	Condition
Workpiece	Al6061 C2680
Punch angle	23.5°
Stamping speed	0.5 mm/min
Stamping depth (Z)	$300, 310, 320, 330, 340, 350, 360, 370, 380\text{ }\mu\text{m}$

The workpiece (Feng An Steel Corporation, Taoyuan, Taiwan) is affixed to the engraving EDM platform with the holder, and the micro punch is mounted on the Z-axis of the EDM machine as shown in Figure 1a. The micro punch stamps the workpiece, and then it moves to the next working point, where the spacing between stamping points is $500\text{ }\mu\text{m}$, as shown in Figure 7b. The workpiece surface is set as the origin, and the punch feeding distance is defined as stamping depth (Z). There are 9 stamping depths at intervals of $10\text{ }\mu\text{m}$ between 300 and $380\text{ }\mu\text{m}$, as shown in Figure 7a.

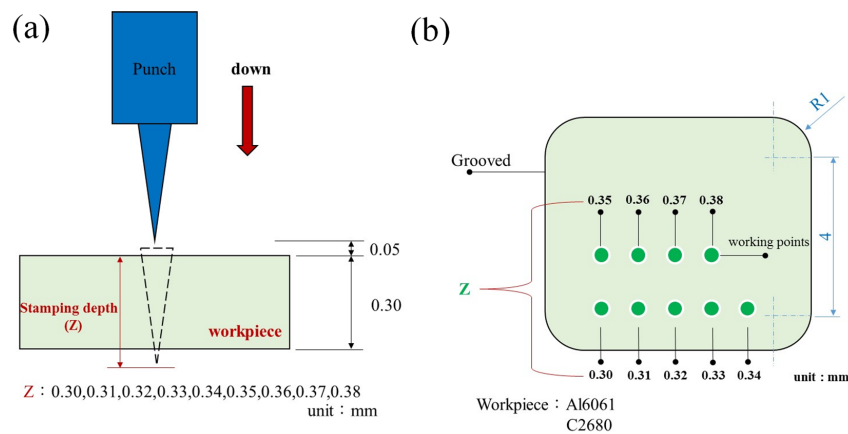


Figure 7. Schematic diagram of processing mode (a) stamping depth definition (b) working point position.

3.2. Laser Processing

The laser processing experiment is as shown in Figure 8a. The laser source is a Nd:YAG laser (LOTIS TII LS-2134UTF, Tokyo Instruments, Inc., Edogawa-ku, Japan) with second harmonic of a 532 nm wavelength. In order to discuss the effect of the defocusing distance on the hole morphology, the focusing lens focal length of 120 mm is changed; The laser processing has not specified the long and short focal lengths. The defocusing distance ranges from $+0.5\text{ mm}$ (positive defocus) to -0.5 mm (negative defocus) with an increment of 0.1 mm , as shown in Figure 8b.

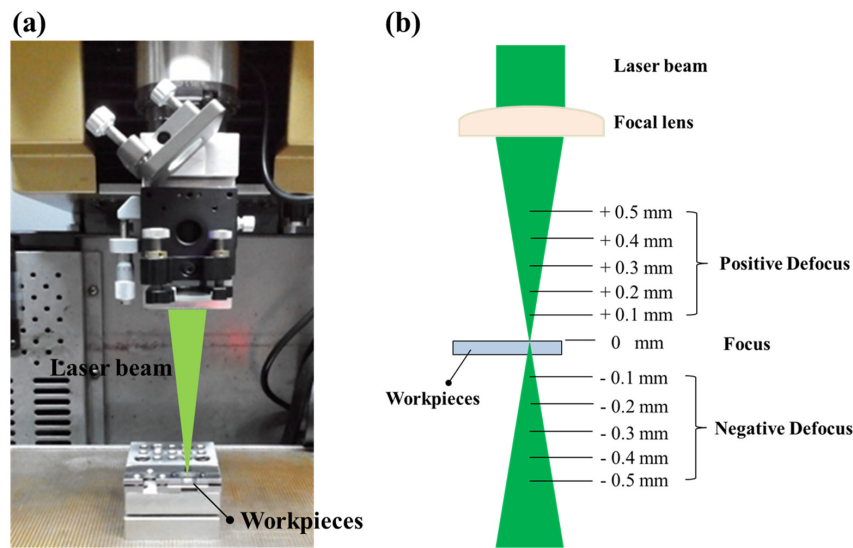


Figure 8. Laser processing experiment (a) laser mechanism (b) laser beam in different focusing arrangements.

The processing parameters of the laser drilling experiment are as shown in Table 3. The sample is the same as the Al6061 sample for the experiment in Section 3.1. The laser powers used in the experiments are 20, 30, 40 mW, which is measured by a powermeter (Ophir-NOVAII, Ophir Optics, Inc., North Andover, MA, USA).

Table 3. Experimental parameters of laser drilling.

Parameter	Condition
Workpieces (Al6061)	300 μ m
Wavelength	532 nm
Frequency	15 Hz
Pumping lamp energy	16, 17, 18 J
Power (Watt)	20, 30, 40 mW
Focal length	120 mm

We will discuss the change of required pulses for perforation, inlet, and outlet diameter with different defocusing distance in the section later.

4. Experimental Results and Discussion

Tool maker’s microscope (OM) and Scanning Electron Microscope (SEM) are used to observe the microhole and micro punch head morphology change and size change before and after stamping. The microhole morphology after stamping is discussed, such as the inlet diameter, the outlet diameter, the influence area diameter, and prominence height. Due to the high aspect ratio of microholes, it is difficult to observe the inside of the microholes, thus, the Wirecut Electrical Discharge Machining (WEDM) cuts close to the edge of microholes, and a following grinding step is used for cross-section observation. We then discuss the microhole wall morphology.

4.1. Microhole Morphology

4.1.1. Micro Stamping

Figure 9 shows the schematic diagram of the microhole geometry definition. The OM photos are as shown in Figure 10. The stamping depth is 380 μ m, and there are goffers around the microhole

entry due to the stamping process. During the process, the materials around the entry is extruded by the stamping head. The stress along the direction of the bevel is in tension, while the direction normal to the bevel is in compression.

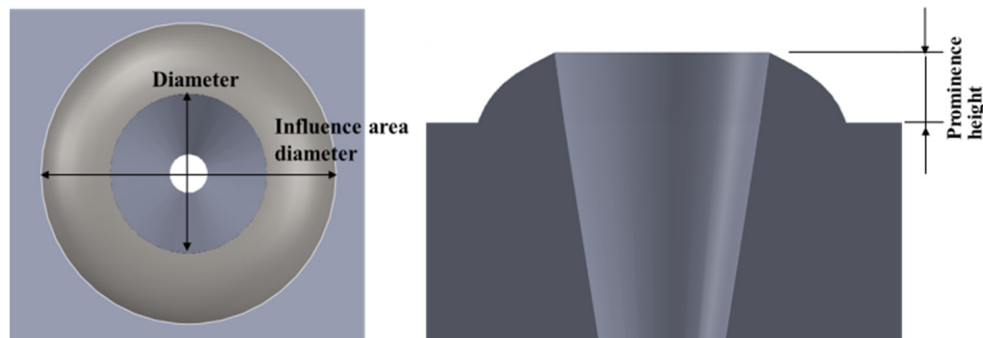


Figure 9. Schematic diagram of hole size measurement.

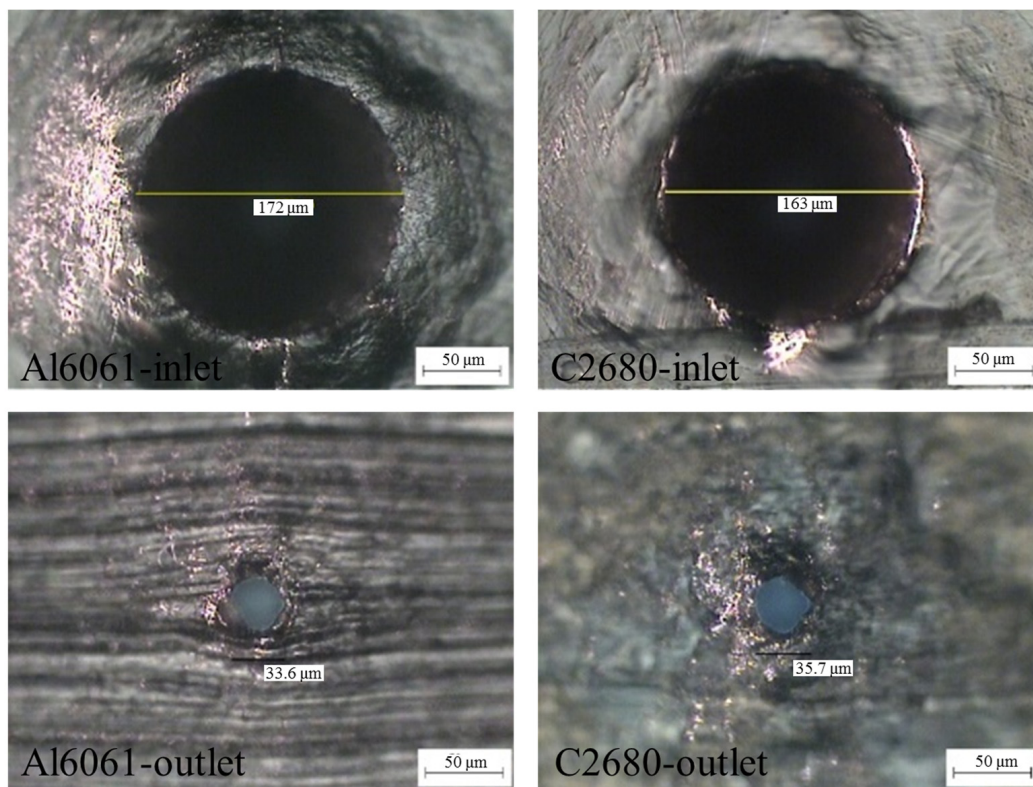


Figure 10. Optical Microscope (OM) images of micro stamping hole morphology ($Z = 380 \mu\text{m}$). Scale bars = $50 \mu\text{m}$.

According to the stamping results, it is observed that the inlet hole is enlarged as the stamping depth increases; this phenomenon is the same in both the Al6061 and C2680; however, the plastic deformation around the inlet of Al6061 is smoother than C2680, as the Al6061 has better plastic deformability.

The inlet diameter and influence area diameter are measured by averaging the measured results in both the X-, Y-axial directions. The prominence height is a distance between the workpiece surface and prominence top and measured by averaging the four point measurements at the top of the prominence. Figure 11 shows that the inlet diameter and prominence height increase linearly as the stamping depth

increases. Meanwhile, the inlet diameter of Al6061 is larger than C2680, and the diameter difference is about 4 μm with the same stamping depth. The prominence height has a linear trend with the inlet diameter, as they are related to each other.

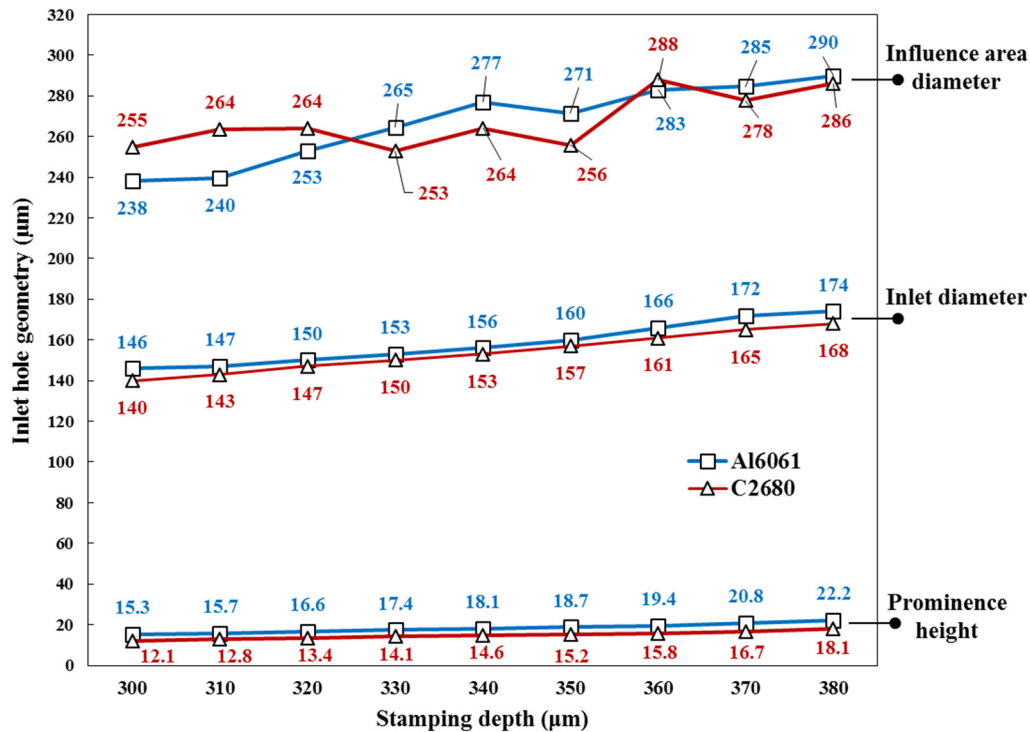


Figure 11. Stamping depth/inlet hole geometry analysis.

The inlet influence area diameter is as shown in Figure 11. The influence area diameter of Al6061 and C2680 workpieces has a nonlinear trend with stamping depth, and because the influence area diameter is formed from material deformation, in which the lattice extrude each other and the material flows laterally due to the V-shaped structure of the hole wall. The influence area diameter is 238–290 μm . The influence area diameter increases with the stamping depth.

The outlet diameter and influence area diameter measurement method is the same as the inlet measurement method. The measurement result is as shown in Figure 12. The stamping results of the two workpieces show that the stamping depth for Al6061 punch forming is 340 μm , whereas, the C2680 stamping depth is only 320 μm . This result matches the inlet forming result. As the C2680 material has higher stiffness, the punching result is better.

The outlet diameter is analyzed in Figure 12. According to the outlet diameters of the two materials, as the punching effect contains rupture and extrusion mechanisms, it is merely ruptured when the perforation begins. The plastic forming stage comes up as the stamping depth increases. Therefore, the larger the outlet size, the better the hole quality. The outlet influence area diameter is approximately the same as the inlet influence area. The influence area diameter increases with stamping depth for both Al6061 and C2680 materials. The prominence height of the outlet increases with the stamping depth; however, the difference is slight, and may be because the plastic deformation resulted from punching is low, at about 5–8 μm .

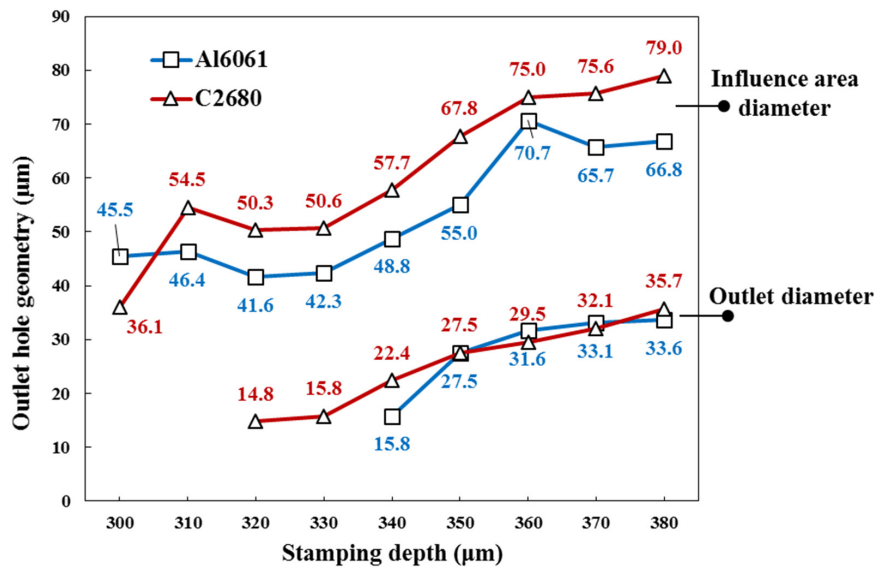


Figure 12. Stamping depth/outlet hole geometry analysis.

4.1.2. Laser Processing

In terms of the experimental parameters of laser drilling, the laser pumping energy is 16, 17, 18 J, and the defocusing distance is +0.5–0.5 mm. Al6061 has a thickness of 300 µm and is perforated by laser thermal ablation. The pulse required for perforation is recorded, and the microhole size is measured.

The inlet and outlet morphologies of the laser processed holes are as shown in Figure 13. When the defocusing distance of the process is increased, the laser focus spot diameter increases, and the depth of the field increases accordingly. When the defocusing distance is +0.1–+0.5 mm, laser energy generates a keyhole due to high power density. Meanwhile, the melted material stack around the keyhole. The Heat affected zone (HAZ) width increases due to the defocusing. When the defocusing distance is –0.1–0.5 mm, the power density of laser is not diffracted along its path as positive defocusing, thus the hole diameter is smaller. Meanwhile, the required number of laser pulse for perforation is less with negative defocusing than with positive defocusing as shown in Figure 14 it shows the relationship between defocusing distance and required pulse number for perforation. The processing time for a focal length of –0.5 mm is the shortest, and may be because the energy density of negative defocus is higher than the positive defocus. The relationship between hole depth and defocusing distance has a similar trend, where the hole depth is inversely proportional to the defocusing distance. As shown in Figure 15, while there is an inlet diameter jump with 18 J laser processing and no obvious change in outlet diameter with 16 J laser processing, the inlet and outlet diameters increases with defocusing distance in other cases. Therefore, the taper angle of holes increases with the defocusing distance. The maximum taper angle is about 9.7°. At the same defocusing distance, a negative defocus results in a larger HAZ width than a positive defocus and it is due to higher energy density.

4.2. Microhole Cross-Section Analysis

In order to obtain the cross-section of holes, WEDM is used to cut across the hole with a following grinding step. As shown in Figure 16b,c, It is observed that the micro tapered hole has good hole wall quality. In the stamping process, the punch head is pressed into the aluminum sheet to form a micro tapered hole, and the flow of the aluminum results in prominence around both the inlet and outlet. The DEFORM-3D simulated result is as shown in Figure 16a. The microhole cross-section by laser processing is as shown in Figure 16d, which shows the irregular cross-section. In addition, the

surface roughness of a microhole cross-section is measured by a 3D surface profiler (NanoFocus μ scan, NanoFocus AG, Oberhausen, Germany).

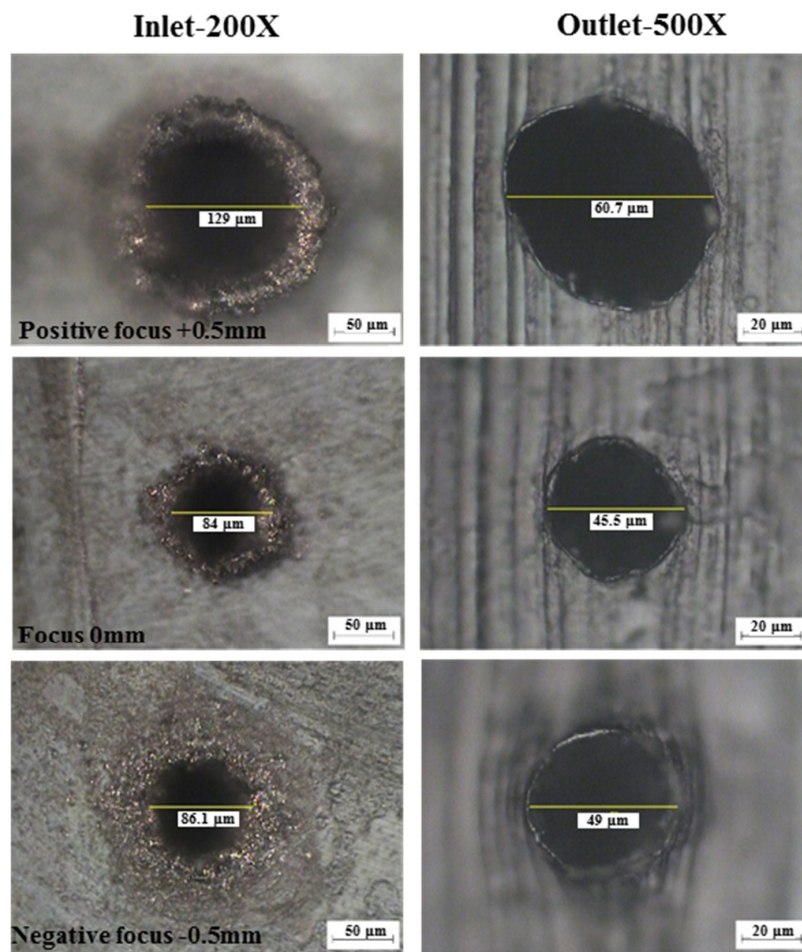


Figure 13. OM images of laser processed holes.

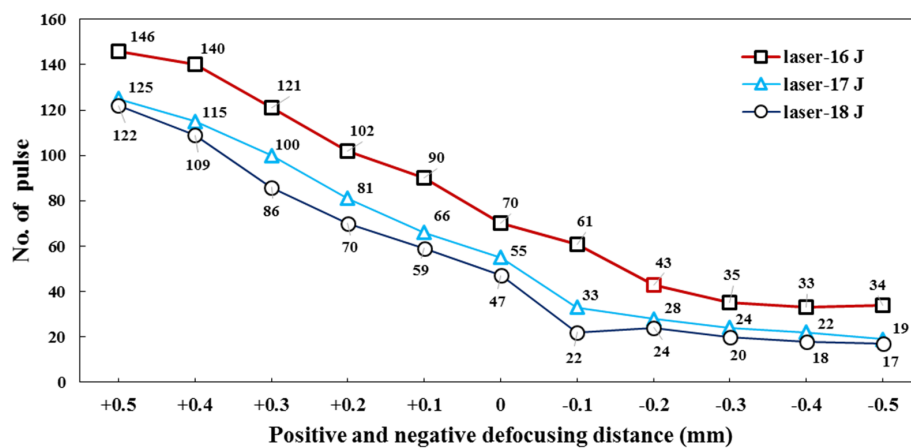


Figure 14. Relationship between positive and negative defocusing distance and pulse number for perforation.

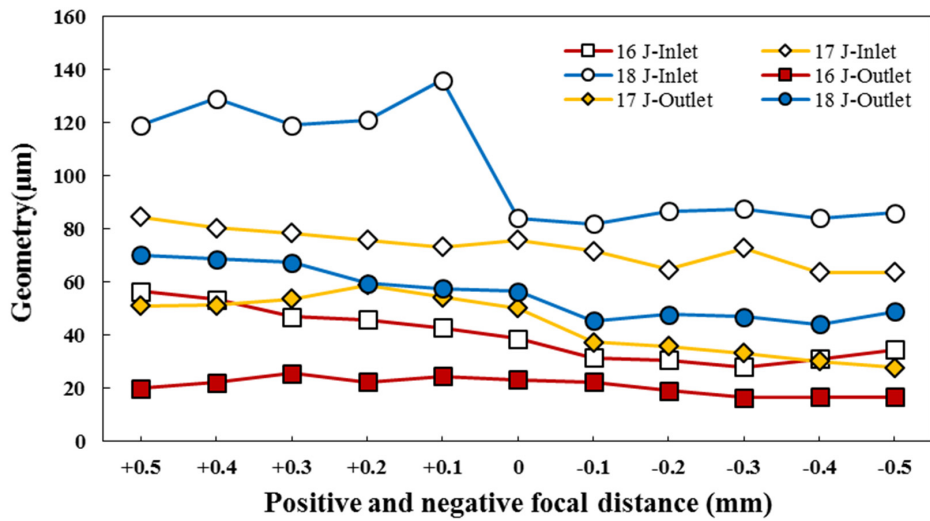


Figure 15. Relationship between positive and negative defocusing distance and diameter.

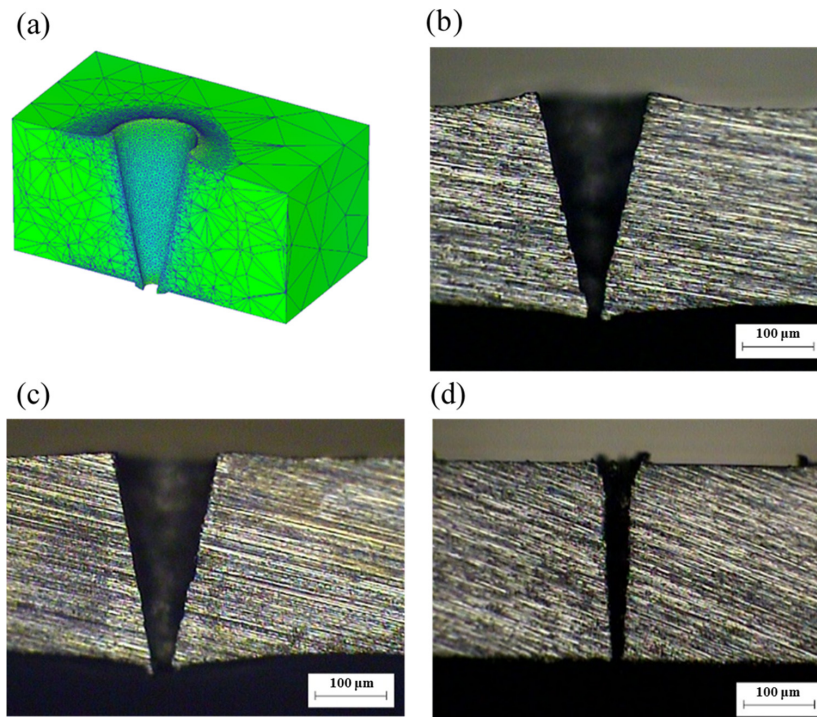


Figure 16. Microhole cross-section (a) simulated view (b) Punch-Al6061 (c) punch-C2680 (d) Laser-Al6061.

We measured the microhole wall morphology along the depth of hole with a length of 200 µm. The result shows the surface is smoother in the microhole by stamping than by laser processing. The surface roughness, Ra, of micro stamping decreases from 1.2 to 0.8 µm, as compared with laser processing. Three holes were measured for each case. Meanwhile, the result shows that surface quality of microholes by stamping can be improved. Moreover, the variation of surface roughness is less than 5% for Al6061 and C2680.

4.3. Punch Morphology after Stamping

The punch head after stamping is as shown in Figure 17. As the punch head is formed by reverse EDM, there are discharge pits and cracks on the surface of the punch head. As the EDM process produces debris, bubbles, and secondary discharge, the punch head tip would be rounded. Therefore, the line contact is produced in the micro stamping process instead of the point contact that causes unbalance and punch head breakage.

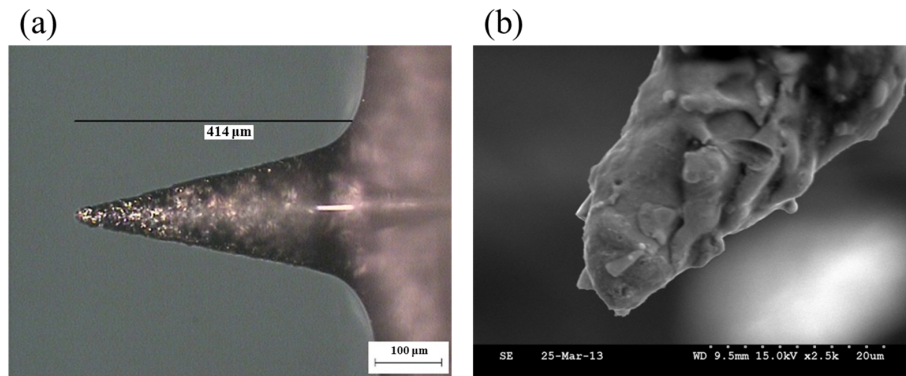


Figure 17. Micro punch head morphology after stamping (a) OM image (b) partially enlarged SEM image.

According to the experimental results, the Al6061 and C2680 workpieces are only punched 18 times with stamping depths of 300–380 μm . Figure 17a is an OM picture of a punch head after stamping and it shows that the punch head is not broken. Figure 17b is a magnified SEM picture of a punch head tip. It shows the punch head is not broken or worn, as the WC has higher strength and wear resistance, and aluminum and copper alloy materials are soft and have high ductility. Therefore, the experimental results prove the feasibility of a tapered punch for micro stamping.

5. Conclusions

This study proposes SWD, and the experimental results prove the feasibility. This method overcomes the bottleneck of a required lower die for micro stamping. The specific conclusions are described as follows:

- (1) We have demonstrated the feasibility of stamping process by a micro-scale tapered punch head and the micro punch head is not apparently worn in the stamping process.
- (2) Micro stamping produces a better micro tapered hole wall quality with Ra value of 0.8 μm than by laser processing.
- (3) The stamping results of Al6061 and C2680 workpieces show that, with the same stamping depth, the prominence height at the inlet of the C2680 is lower than Al6061 (~20%). The results show that the C2680 workpiece has better micro tapered hole wall quality than Al6061.
- (4) The required tapered hole morphology and size can be accurately obtained by controlling the stamping depth. The inlet and outlet diameter of microholes can be adjusted by the stamping depth or punch head angle.
- (5) The micro tapered hole depth is 300 μm , and the maximum ratio of inlet to outlet diameter is 18:1.
- (6) Laser processing is used to form tapered holes. Although the energy and defocusing distance can be adjusted, the largest taper angle in the experiments was 9.7° , which was smaller than the angle of 23.5° produced by the stamping process.
- (7) The surface roughness of micro stamping is 33% lower than laser processing.
- (8) SWD, as proposed in this study, can make the required taper angle by changing the punch angle.

While reverse EDM used in this experiment is a low throughput process, grinding punch head is an alternative method and can be used for mass production.

Acknowledgments: The authors would like to acknowledge the financial support provided by Ministry of Science and Technology, China (Taiwan) (103-2221-E-027-135-MY2).

Author Contributions: Yung-Chou Hung, Chao-Ching Ho and Chia-Lung Kuo performed the experiment and data analysis work; Yung-Chou Hung, Jin-Chen Hsu and Yuan-Jen Chang wrote the manuscript; Jin-Chen Hsu, Chao-Ching Ho, Chia-Lung Kuo and Yuan-Jen Chang contributed revision of this paper.

Conflicts of Interest: The authors declare no conflict of interest.

References

1. Derzija, B.H.; Izet, B. Experimental and numerical investigation of temperature distribution and hole geometry during laser drilling process. *Procedia Eng.* **2015**, *100*, 384–393.
2. Ahn, D.G.; Jung, G.W. Influence of process parameters on drilling characteristics of Al 1050 sheet with thickness of 0.2 mm using pulsed Nd:YAG laser. *Trans. Nonferr. Met. Soc. China* **2009**, *19*, s157–s163. [[CrossRef](#)]
3. Yao, K.C.; Lin, J. The characterization of the hole-contour and plume ejection in the laser drilling with various inclination angles. *Opt. Laser Technol.* **2013**, *48*, 110–116. [[CrossRef](#)]
4. Masuzawa, T.; Fujino, M.; Kobayashi, K. Wire electro-discharge grinding for micro-machining. *CIRP Ann. Manuf. Technol.* **1985**, *34*, 431–434. [[CrossRef](#)]
5. Fujino, M.; Yamamoto, M.; Masuzawa, T. *Micro-Punching System as an Application of WEDG*; Institute of Industrial Science, The University of Tokyo SEISAN-KENKYU: Tokyo, Japan, 1987; Volume 39, pp. 277–280. (In Japanese)
6. Chern, G.L.; Wang, S.D. Punching of noncircular micro-holes and development of micro-forming. *Precis. Eng.* **2007**, *31*, 210–217. [[CrossRef](#)]
7. Joo, B.Y.; Oh, S.I.; Jeon, B.H. Development of micro punching system. *CIRP Ann. Manuf. Technol.* **2001**, *50*, 191–194. [[CrossRef](#)]
8. Joo, B.Y.; Rhim, S.H.; Oh, S.I. Micro-hole fabrication by mechanical punching process. *J. Mater. Process. Technol.* **2005**, *170*, 593–601. [[CrossRef](#)]
9. Hwang, Y.L.; Kuo, C.L.; Hwang, S.F. Fabrication of a micro-pin array with high density and high hardness by combining mechanical peck-drilling and reverse-EDM. *J. Mater. Process. Technol.* **2010**, *210*, 1103–1130. [[CrossRef](#)]
10. Xu, J.; Guo, B.; Shan, D.; Wang, C.; Li, J.; Liu, Y.; Qu, D. Development of a micro-forming system for micro-punching process of micro-hole arrays in brass foil. *J. Mater. Process. Technol.* **2012**, *212*, 2238–2246. [[CrossRef](#)]
11. Kibe, Y.; Okada, Y.; Mitsui, K. Machining accuracy for shearing process of thin-sheet metals—Development of initial tool position adjustment system. *Int. J. Mach. Tools Manuf.* **2007**, *47*, 1728–1737. [[CrossRef](#)]
12. Oh, S.I.; Wu, W.T.; Tang, J.P. Simulations of cold forging processes by the DEFORM system. *J. Mater. Process. Technol.* **1992**, *35*, 357–370. [[CrossRef](#)]
13. Nagao, Y.; Knoerr, M.; Altan, T. Improvement of tool life in cold forging of complex automotive parts. *J. Mater. Process. Technol.* **1994**, *46*, 73–85. [[CrossRef](#)]
14. Kim, H.; Sweeney, K.; Altan, T. Application of computer aided simulation to investigate metal flow in selected forging operations. *J. Mater. Process. Technol.* **1994**, *46*, 127–154. [[CrossRef](#)]
15. Kim, H.H.; Kang, C.G. Numerical simulation and experimental study for rheo-forged component using direct and indirect die system. *Trans. Nonferr. Met. Soc. China* **2010**, *20*, 1799–1804. [[CrossRef](#)]



© 2016 by the authors; licensee MDPI, Basel, Switzerland. This article is an open access article distributed under the terms and conditions of the Creative Commons by Attribution (CC-BY) license (<http://creativecommons.org/licenses/by/4.0/>).